

Energy transport in the near field of an electric dipole near a layer of material

Henk F. Arnoldus* and Matthew J. Berg

Department of Physics and Astronomy, Mississippi State University, P.O. Drawer 5167, Mississippi State, Mississippi, 39762-5167, USA

(Received 22 August 2014; accepted 25 September 2014)

We consider an oscillating electric dipole, embedded in a uniform medium with relative permittivity ϵ_1 and relative permeability μ_1 . The dipole is located near an interface with a layer with uniform material parameters ϵ_2 and μ_2 , and the second interface borders a uniform medium with parameters ϵ_3 and μ_3 . We have obtained the solutions for the electric and magnetic fields in the various regions, without any restrictions on the parameters and for any state of oscillation of the dipole (elliptical, in general). The solution involves a set of auxiliary functions, which are given as integral representations containing the Fresnel coefficients for plane waves. With this solution, the field lines of energy flow can be obtained, and we have considered the flow pattern for the simple case of a dipole oscillating perpendicular to the interface. When the material of the layer is optically thicker than the embedding medium of the dipole, energy flows more or less along straight lines. At an interface, the field lines refract, similar to optical rays. When the layer material is optically thinner, the energy flow lines curve. A portion of the energy that propagates toward the interface bends away from it before reaching the interface. Other field lines of energy flow cross the interface, but then return to the area of the dipole by crossing the interface again. This leads to an oscillation of energy back and forth through the interface. In the neighborhood of this oscillation, a concentric set of vortex tori appears.

Keywords: dipole radiation; reflection; transmission; Fresnel coefficients; angular spectrum; Poynting vector

1. Introduction

An oscillating electric dipole near an interface was considered for the first time by Sommerfeld [1], who studied the propagation of the emitted electromagnetic waves near the surface of the Earth. Ever since then, a large number of publications have been devoted to this topic. The radiation field can most easily be computed by means of the Green's function for the configuration or an angular spectrum representation, and these methods apply both to a single interface and multiple parallel interfaces (slabs of material) [2–6]. In such an approach, the electric and magnetic fields are found as integral representations involving the Fresnel coefficients. The reflected and transmitted far fields can then be obtained by asymptotic expansion, and the radiated power per unit solid angle can be found in closed form [7]. Interestingly, the total emitted power is altered by the presence of the interface, as compared to the emitted power by the same dipole in free space. When the radiation is electric dipole radiation emitted during an electronic transition in an atom or molecule, it implies that the lifetime of the excited state is influenced by the interaction of the radiation with the interface. This change in emission rate and lifetime has been computed for various configurations, and has been observed experimentally [8–12]. Most notably, the change in emission rate depends on the distance between

the particle and the interface, assuming this distance is of the order of a wavelength.

The change in emission rate and power per unit solid angle are macroscopic effects, observable in the far field. In near-field optics, the details of the radiation field in the vicinity of the source are of interest, and this requires an exact solution to Maxwell's equations. Radiation patterns have intricate sub-wavelength structures, including interference vortices and singularities [13], and the angular emission pattern of the radiation (which is not the same as the power per unit solid angle in the far field) is drastically altered due to the presence of the interface [14]. When electric dipole radiation passes through an interface into a thinner medium, some of the energy oscillates back and forth through the interface [15]. We shall consider the arrangement shown in Figure 1. An electric dipole, oscillating at angular frequency ω , is embedded in a uniform medium with relative permittivity ϵ_1 and relative permeability μ_1 , and is located on the z axis, a distance H from the xy plane. The planes $z = 0$ and $z = L$ are interfaces between media with different ϵ and μ , as shown in the figure. The values of ϵ and μ depend on ω , and are in general complex with a non-negative imaginary part. The (point-like) oscillating electric dipole has a dipole moment

$$\mathbf{d}(t) = d_o \text{Re}[\mathbf{u} \exp(-i\omega t)], \quad d_o > 0, \quad \mathbf{u} \cdot \mathbf{u}^* = 1. \quad (1)$$

*Corresponding author. Email: hfal@msstate.edu

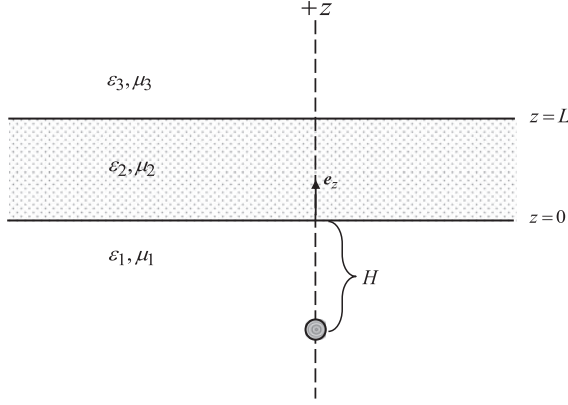


Figure 1. Shown here is the arrangement we consider. The electric dipole is located on the negative z axis, a distance H from the xy plane. The second interface is the plane $z = L$, and the three media have relative permittivities ϵ_i and relative permeabilities μ_i as shown.

In its most general state of oscillation, the dipole moment $\mathbf{d}(t)$ traces out an ellipse in a plane [16]. For instance, if we take

$$\mathbf{u} = -(\mathbf{e}_x + i\mathbf{e}_y)/\sqrt{2}, \quad (2)$$

then the dipole moment traces out a circle in the xy plane, and the rotation is counterclockwise when viewed from the positive z axis. Energy is emitted as a vortex structure, with the field lines of energy flow spiraling around the z axis [17,18]. The arrangement in Figure 1 has also been considered in Ref. [19] for $\mathbf{u} = \mathbf{e}_z$, a vertical dipole, and $\mathbf{u} = \mathbf{e}_x$, a horizontal dipole. We shall obtain the solution for arbitrary \mathbf{u} , and illustrate the flow of energy through this system with examples.

2. Electric dipole radiation

When the dipole oscillates with angular frequency ω , the electric and magnetic fields also oscillate with the same angular frequency. For the electric field at field point \mathbf{r} we write

$$\mathbf{E}(\mathbf{r}, t) = \text{Re}[\mathbf{E}(\mathbf{r}) \exp(-i\omega t)], \quad (3)$$

with $\mathbf{E}(\mathbf{r})$ being the complex amplitude, and the magnetic field $\mathbf{B}(\mathbf{r}, t)$ is represented similarly. We shall refer to $\mathbf{E}(\mathbf{r})$ as the electric field, rather than $\mathbf{E}(\mathbf{r}, t)$. It is convenient to split off overall factors as

$$\mathbf{E}(\mathbf{r}) = \zeta \tilde{\mathbf{E}}(\mathbf{r}), \quad (4)$$

$$\mathbf{B}(\mathbf{r}) = \frac{\zeta}{c} \tilde{\mathbf{B}}(\mathbf{r}), \quad (5)$$

with

$$\zeta = \frac{\mu_1 k_o^3 d_o}{4\pi\epsilon_o}, \quad (6)$$

and $k_o = \omega/c$, the free-space wavenumber. The frequency dependence can be scaled away entirely by adopting dimensionless variables. We set $h = k_o H$ for the distance between the dipole and the interface and $\ell = k_o L$ for the layer thickness. The dimensionless position vector of the field point \mathbf{r} with respect to the location of the dipole is then $\mathbf{q}_1 = k_o \mathbf{r} + h\mathbf{e}_z$. For the radiation emitted by the dipole we have

$$\begin{aligned} \tilde{\mathbf{E}}_d(\mathbf{r}) &= \left\{ \mathbf{u} - (\hat{\mathbf{q}}_1 \cdot \mathbf{u})\hat{\mathbf{q}}_1 + [\mathbf{u} - 3(\hat{\mathbf{q}}_1 \cdot \mathbf{u})\hat{\mathbf{q}}_1] \frac{i}{n_1 q_1} \left(1 + \frac{i}{n_1 q_1} \right) \right\} \\ &\quad \times \frac{\exp(in_1 q_1)}{q_1}, \end{aligned} \quad (7)$$

$$\tilde{\mathbf{B}}_d(\mathbf{r}) = n_1 (\hat{\mathbf{q}}_1 \times \mathbf{u}) \left(1 + \frac{i}{n_1 q_1} \right) \frac{\exp(in_1 q_1)}{q_1}, \quad (8)$$

with $q_1 = |\mathbf{q}_1|$ and $\hat{\mathbf{q}}_1 = \mathbf{q}_1/q_1$. The index of refraction of medium i is the solution of

$$n_i^2 = \epsilon_i \mu_i, \quad \text{Im } n_i > 0, \quad i = 1, 2, 3. \quad (9)$$

This leaves an ambiguity when ϵ_i and μ_i are either both positive or both negative. In these cases, the solution should be considered with a limit, where at first small imaginary parts are included in ϵ_i and μ_i . For ϵ_i and μ_i as both positive we should take the root $n_i > 0$, and for ϵ_i and μ_i as both negative we have $n_i < 0$ (negative index of refraction material).

3. Angular spectrum

With Weyl's representation of the scalar Green's function, the electric dipole field can be represented by an angular spectrum of plane waves [20]. The representation depends on whether $z > -H$ (above the dipole in Figure 1) or $z < -H$ (below the dipole). The source field in $z > -H$ serves as the incident field on the interface, so we shall consider only this case. The angular spectrum is an integral representation, with the integral running over the \mathbf{k}_\parallel plane. This is a fictitious plane, parallel to the xy plane. For a given \mathbf{k}_\parallel , a plane wave has wave vector

$$\mathbf{k} = \mathbf{k}_\parallel + k_o v_1 \mathbf{e}_z. \quad (10)$$

Its z component, $k_o v_1$, is determined by the dispersion relation in medium 1. First, we set

$$\alpha = k_\parallel / k_o, \quad (11)$$

with k_\parallel being the magnitude of \mathbf{k}_\parallel . Then, v_1 must be the solution of

$$v_1^2 = n_1^2 - \alpha^2, \quad \text{Im } v_1 > 0. \quad (12)$$

We take the root with $\text{Im } \nu_1 > 0$ because of causality. For $n_1^2 > 0$ this leaves an ambiguity in the solution, and we shall assume that an appropriate limit is considered, just like for the index of refraction. For the common case of ε_1 and μ_1 as both positive, ν_1 is positive for $\alpha < n_1$ (traveling wave) and positive imaginary for $\alpha > n_1$ (evanescent wave). For the dipole field we have

$$\tilde{\mathbf{E}}_d(\mathbf{r}) = \frac{i}{2\pi k_o^2} \int d^2 \mathbf{k}_{\parallel} \frac{\exp(ih\nu_1)}{\nu_1} \exp(i\mathbf{k} \cdot \mathbf{r}) \left[\mathbf{u} - \frac{1}{n_1^2 k_o^2} (\mathbf{u} \cdot \mathbf{k}) \mathbf{k} \right], \quad (13)$$

and the magnetic field follows from

$$\mathbf{B}(\mathbf{r}) = -\frac{i}{\omega} \nabla \times \mathbf{E}(\mathbf{r}). \quad (14)$$

For a given \mathbf{k}_{\parallel} , we set

$$\mathbf{e}_s = \frac{1}{\alpha k_o} \mathbf{e}_z \times \mathbf{k}_{\parallel}, \quad (15)$$

$$\mathbf{e}_p = \frac{1}{n_1 k_o} \mathbf{k} \times \mathbf{e}_s, \quad (16)$$

which are unit polarization vectors for s and p waves. The electric field then becomes

$$\tilde{\mathbf{E}}_d(\mathbf{r}) = \frac{i}{2\pi k_o^2} \sum_{\sigma} \int d^2 \mathbf{k}_{\parallel} \frac{\exp(ih\nu_1)}{\nu_1} (\mathbf{u} \cdot \mathbf{e}_{\sigma}) \mathbf{e}_{\sigma} \exp(i\mathbf{k} \cdot \mathbf{r}), \quad (17)$$

with $\sigma = s, p$.

4. Method of solution

The representation (17) of the electric dipole field is a superposition of plane waves with wave vector \mathbf{k} and polarization σ . Each plane wave, with a given \mathbf{k}_{\parallel} and σ , is

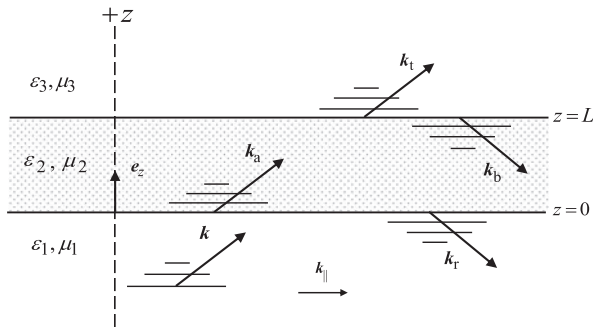


Figure 2. Schematically shown here are the various waves for the plane-wave solution for the layer problem. Each wave vector must have the same parallel component, \mathbf{k}_{\parallel} . Their z components, however, are determined by the dispersion relations of the materials and by causality. The waves can be traveling, evanescent, or a combination of both. The arrows indicate the wave vector when the wave is pure traveling, and the lines indicate the direction of exponential decay if the wave is pure evanescent.

a solution of Maxwell's equations in medium 1 for $z > -H$. Such a plane wave reflects at the $z = 0$ interface, and partially transmits into the layer. This transmitted wave reflects at the $z = L$ interface, and partially transmits into region 3. The wave vectors for the various waves are shown in Figure 2. Each wave vector must have the same \mathbf{k}_{\parallel} as the incident wave, due to the boundary conditions. The perpendicular components of the wave vectors are determined by the dispersion relations in the media and by causality. Each plane wave has the same polarization σ as the incident wave. The complex amplitudes of the waves, relative to the incident wave, are expressed as Fresnel coefficients, and these will be indicated by R_{σ} , $D_{a\sigma}$, $D_{b\sigma}$, and T_{σ} , in obvious notation. Their expressions and sign conventions are given in Appendix 1. They depend parametrically on the respective values of ε and μ , and the dimensionless layer thickness ℓ , and are functions of the variable α , defined by Equation (11).

The fields in the various regions are in the same superpositions as the incident waves in Equation (17). In $z < 0$, region 1, the field is the sum of the dipole field and the reflected field

$$\tilde{\mathbf{E}}_1(\mathbf{r}) = \tilde{\mathbf{E}}_d(\mathbf{r}) + \tilde{\mathbf{E}}_r(\mathbf{r}), \quad (18)$$

with $\tilde{\mathbf{E}}_d(\mathbf{r})$ given by Equation (7). In region 2, $0 < z < L$, we have

$$\tilde{\mathbf{E}}_2(\mathbf{r}) = \tilde{\mathbf{E}}_a(\mathbf{r}) + \tilde{\mathbf{E}}_b(\mathbf{r}), \quad (19)$$

and in region 3, $z > L$, we only have the transmitted field

$$\tilde{\mathbf{E}}_3(\mathbf{r}) = \tilde{\mathbf{E}}_t(\mathbf{r}). \quad (20)$$

The same holds for the corresponding magnetic fields.

For instance, the reflected electric field is given by

$$\tilde{\mathbf{E}}_r(\mathbf{r}) = \frac{i}{2\pi k_o^2} \sum_{\sigma} \int d^2 \mathbf{k}_{\parallel} \frac{\exp(ih\nu_1)}{\nu_1} (\mathbf{u} \cdot \mathbf{e}_{\sigma}) R_{\sigma} \mathbf{e}_{r\sigma} \exp(i\mathbf{k}_r \cdot \mathbf{r}). \quad (21)$$

The polarization vectors $\mathbf{e}_{r\sigma}$ and the wave vector \mathbf{k}_r are defined in Appendix 1. We shall use cylindrical coordinates (ρ, ϕ, z) for the field point \mathbf{r} . The corresponding basis vectors are

$$\mathbf{e}_{\rho} = \mathbf{e}_x \cos \phi + \mathbf{e}_y \sin \phi, \quad (22)$$

$$\mathbf{e}_{\phi} = -\mathbf{e}_x \sin \phi + \mathbf{e}_y \cos \phi, \quad (23)$$

together with \mathbf{e}_z . In the \mathbf{k}_{\parallel} plane, we adopt polar coordinates as follows. For a given field point \mathbf{r} , the vectors \mathbf{e}_{ρ} and \mathbf{e}_{ϕ} are fixed in the xy plane. In the \mathbf{k}_{\parallel} plane, we take the \tilde{x} and \tilde{y} axes along \mathbf{e}_{ρ} and \mathbf{e}_{ϕ} , respectively, and $(k_{\parallel}, \tilde{\phi})$ then represent the polar coordinates of \mathbf{k}_{\parallel} with respect to the \tilde{x} and \tilde{y} axes in the usual way. So we have

$$\mathbf{k}_{\parallel} = k_{\parallel} (\mathbf{e}_{\rho} \cos \tilde{\phi} + \mathbf{e}_{\phi} \sin \tilde{\phi}), \quad (24)$$

and $k_{\parallel} = \alpha k_o$ with Equation (11). The integral over the \mathbf{k}_{\parallel} plane then becomes

$$\int d^2 \mathbf{k}_{\parallel}(\dots) = k_o^2 \int_0^{\infty} d\alpha \alpha \int_0^{2\pi} d\tilde{\phi}(\dots). \quad (25)$$

With $\mathbf{r} = \rho \mathbf{e}_{\rho} + z \mathbf{e}_z$ and $\mathbf{k}_r = \mathbf{k}_{\parallel} - k_o v_1 \mathbf{e}_z$ we have $\mathbf{k}_r \cdot \mathbf{r} = \rho k_{\parallel} \cos \tilde{\phi} - k_o v_1 z$. We introduce dimensionless coordinates as $\bar{x} = k_o x$, $\bar{y} = k_o y$, $\bar{z} = k_o z$ and $\bar{\rho} = k_o \rho$. In these coordinates, 2π corresponds to one free-space optical wavelength. We have $\mathbf{k}_r \cdot \mathbf{r} = \alpha \bar{\rho} \cos \tilde{\phi} - v_1 \bar{z}$, which depends on the integration variable $\tilde{\phi}$. The remaining $\tilde{\phi}$ dependence only enters through the polarization vectors \mathbf{e}_{σ} and $\mathbf{e}_{r,\sigma}$. We find

$$\mathbf{e}_s = \mathbf{e}_{rs} = \mathbf{e}_{\phi} \cos \tilde{\phi} - \mathbf{e}_{\rho} \sin \tilde{\phi}, \quad (26)$$

$$\mathbf{e}_p = \frac{1}{n_1} (\alpha \mathbf{e}_z - v_1 \mathbf{e}_{\rho} \cos \tilde{\phi} - v_1 \mathbf{e}_{\phi} \sin \tilde{\phi}), \quad (27)$$

$$\mathbf{e}_{rp} = \frac{1}{n_1} (\alpha \mathbf{e}_z + v_1 \mathbf{e}_{\rho} \cos \tilde{\phi} + v_1 \mathbf{e}_{\phi} \sin \tilde{\phi}). \quad (28)$$

In the integrand in Equation (21) we have $(\mathbf{u} \cdot \mathbf{e}_{\sigma}) \mathbf{e}_{r\sigma}$, with a summation over σ , so this leads to a large number of terms. Each term contains the factor $\exp(i\alpha \bar{\rho} \cos \tilde{\phi})$ and combinations of $\sin \tilde{\phi}$ and $\cos \tilde{\phi}$. The integrals over $\tilde{\phi}$ can be expressed in terms of Bessel functions. For instance,

$$\int_0^{\infty} d\tilde{\phi} \exp(i\alpha \bar{\rho} \cos \tilde{\phi}) \sin^2 \tilde{\phi} = \pi [J_0(\alpha \bar{\rho}) + J_2(\alpha \bar{\rho})]. \quad (29)$$

Then Equation (21) becomes

$$\tilde{\mathbf{E}}_r(\mathbf{r}) = \frac{i}{2} (\mathbf{u} \cdot \mathbf{e}_{\rho}) \mathbf{e}_{\rho} \int_0^{\infty} d\alpha \frac{\alpha}{v_1} \exp[iv_1(h - \bar{z})] R_s(J_0 + J_2) + \text{many more terms.} \quad (30)$$

The argument of each Bessel functions is $\alpha \bar{\rho}$ and R_s is a function of α . The function v_1 also depends on α . Then we introduce the auxiliary function

$$R_s^{(1)}(\bar{\rho}, \bar{z}) = \frac{i}{2} \int_0^{\infty} d\alpha \frac{\alpha}{v_1} \exp[iv_1(h - \bar{z})] R_s(J_0 + J_2), \quad (31)$$

which gives

$$\tilde{\mathbf{E}}_r(\mathbf{r}) = \mathbf{e}_{\rho} (\mathbf{u} \cdot \mathbf{e}_{\rho}) R_s^{(1)}(\bar{\rho}, \bar{z}) + \text{many more terms.} \quad (32)$$

With this method the fields in all regions can be obtained. The fields can be expressed entirely in terms of auxiliary functions $R_{\sigma}^{(m)}$, $D_{k\sigma}^{(m)}$, and $T_{\sigma}^{(m)}$, with $\sigma = s, p$, $k = a, b$, and $m = 1, 2, \dots$. These functions depend on the dimensionless field point coordinates $\bar{\rho}$ and \bar{z} , and parametrically on ℓ and h , and on the respective values of ε and μ . They are defined in Appendix 2, and the expressions for the fields are given in Appendix 3.

5. Traveling and evanescent parts

In this section, we shall consider the common case where ε_1 and μ_1 are both positive, so that n_1 is positive. The angular spectrum representation (17) of the incident field $\tilde{\mathbf{E}}_d(\mathbf{r})$ has a factor $1/v_1$ in the integrand. We see from Equation (12) that $v_1 = 0$ for $\alpha = n_1$, and this point is on the integration axis for the integration over α in the auxiliary functions in Appendix 2. When ε_1 and μ_1 are not both positive this is not an issue, since the branch point then has an imaginary part, and is off the integration axis. As shown in Appendix 2, this factor of $1/v_1$ cancels for a , b , and t waves, since the corresponding Fresnel coefficients are proportional to v_1 . However, for five of the $R_{\sigma}^{(m)}$'s this factor is present, and therefore the integration runs over the singularity at $\alpha = n_1$. The singularity is integrable, but it is numerically not attractive to have such a complication. Fortunately, this singularity can be removed by a change of variables. To this end, we split the range of integration in $0 < \alpha < n_1$ and $n_1 < \alpha < \infty$. In the first range, the incident waves are traveling, and in the second the incident waves are evanescent. For traveling waves we make the substitution $t = (n_1^2 - \alpha^2)^{1/2}$, which gives

$$\int_0^{n_1} d\alpha \frac{\alpha}{v_1}(\dots) = \int_0^{n_1} dt(\dots). \quad (33)$$

For evanescent waves we set $t = (\alpha^2 - n_1^2)^{1/2}$, which yields

$$\int_{n_1}^{\infty} d\alpha \frac{\alpha}{v_1}(\dots) = -i \int_0^{\infty} dt(\dots). \quad (34)$$

In the integrations over t , the $1/v_1$ singularity has disappeared.

Figure 3 shows the real and imaginary parts of the reflection coefficient R_p as a function of α . We notice a

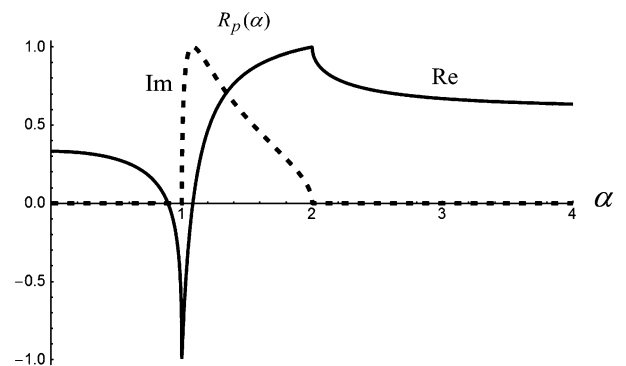


Figure 3. The solid and dashed curves here represent the real and imaginary parts, respectively, of the Fresnel reflection coefficient for a p -polarized wave as a function of α . The parameters are $\varepsilon_1 = 1$, $\mu_1 = 1$, $\varepsilon_3 = 4$, $\mu_3 = 1$, and $\ell = 0$. The indices of refraction are $n_1 = 1$ and $n_2 = 2$. Note that the real part has a sharp peak at the index of refraction $\alpha = n_1$.

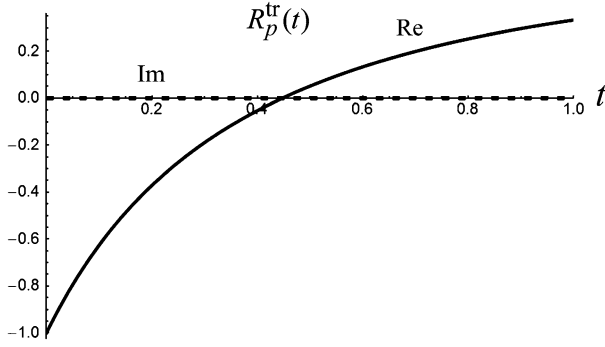


Figure 4. Shown here are the real and imaginary parts of the same reflection coefficient as in Figure 3, for the range $0 < \alpha < n_1$ (traveling waves). Here, the independent variable is t , rather than α , and we see that the sharp peak in the real part seen in Figure 3 has disappeared.

sharp peak in the real part at $\alpha = n_1$, which is the borderline point between traveling and evanescent waves. When we transform to t as the independent variable, as in the previous paragraph, then the functional dependence of R_p is altered. Figures 4 and 5 show R_p in the traveling and evanescent regime, respectively, as a function of t . The point $\alpha = n_1$ transforms to the point $t = 0$ in both regimes, and we see that as a function of t , the reflection coefficient no longer has a sharp peak. The other Fresnel coefficients have a similar peak at $\alpha = n_1$, and they also disappear in the transformation. Therefore, it seems numerically advantageous to split all the integrals.

The splitting of the integrals over α in the auxiliary functions removes the $1/v_1$ singularity in five of these functions. The other functions do not have this singularity, but the splitting smooths the Fresnel coefficients. The trade-off here is that this doubles the number of integrals to be computed for each field point.

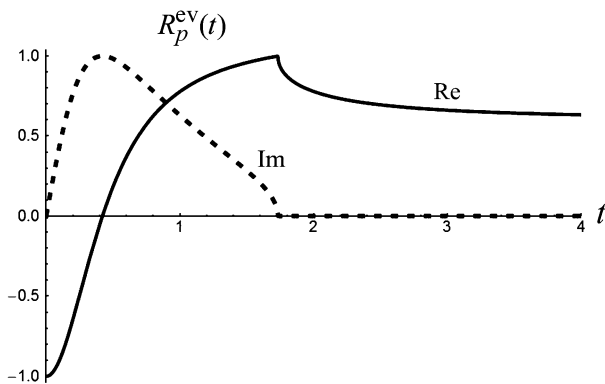


Figure 5. Shown here are the real and imaginary parts of the same reflection coefficient as in Figure 3, for the range $\alpha > n_1$ (evanescent waves). When seen as a function of t , the sharp peak in the real part disappears.

6. Energy flow lines

Electromagnetic energy flows along the field lines of the Poynting vector. The time averaged (over an optical cycle) Poynting vector is defined as

$$\mathcal{S}_i(\mathbf{r}) = \frac{1}{2\mu_o} \operatorname{Re} \frac{1}{\mu_i} \mathbf{E}_i(\mathbf{r})^* \times \mathbf{B}_i(\mathbf{r}), \quad i = 1, 2, 3, \quad (35)$$

and here i numbers the three regions. We split off an overall factor as

$$\mathcal{S}_i(\mathbf{r}) = \frac{|\zeta|^2}{2\mu_o c} \tilde{\mathcal{S}}_i(\mathbf{r}), \quad (36)$$

which gives

$$\tilde{\mathcal{S}}_i(\mathbf{r}) = \operatorname{Re} \frac{1}{\mu_i} \tilde{\mathbf{E}}_i(\mathbf{r})^* \times \tilde{\mathbf{B}}_i(\mathbf{r}), \quad (37)$$

in terms of the dimensionless field amplitudes. Although written as a function of \mathbf{r} , this vector only depends on the dimensionless position vector \mathbf{q} , corresponding to a field point with dimensionless coordinates \bar{x} , \bar{y} , and \bar{z} . Let $\mathbf{q}(t)$ be a parametrization of a field line through a given point \mathbf{q}_o in region i . Then $\mathbf{q}(t)$ is a solution of

$$\frac{d}{dt} \mathbf{q}(t) = \tilde{\mathcal{S}}_i(\mathbf{q}). \quad (38)$$

This equation requires numerical integration, starting from the initial point \mathbf{q}_o .

Field lines of a vector field are determined by the directions of the vectors at the field points, but not by their magnitudes. Therefore, $\tilde{\mathcal{S}}_i$ and $f(\mathbf{q})\tilde{\mathcal{S}}_i$, with $f(\mathbf{q})$ as a positive function of \mathbf{q} , have the same field lines. The electric and magnetic dipole fields, Equations (7) and (8), respectively, have singularities at the location of the dipole ($q_1 = 0$), and this may give rise to numerical problems when integrating Equation (38) in the neighborhood of the dipole. We multiply the electric fields through by q_1^3 and the magnetic fields by q_1^2 . Then the source fields remain finite at $q_1 = 0$, and this greatly improves the numerical accuracy.

7. Vertical dipole

The solution for the fields in the various regions is given in Appendix 3, with the auxiliary functions defined in Appendix 2. For the most general solution (arbitrary \mathbf{u}), a large number of auxiliary functions must be computed for each field point, and when we split the integrals into traveling and evanescent parts, this number doubles. The numerical integration of Equation (38), after multiplying through by q_1^3 and q_1^2 for the electric and magnetic fields, respectively, requires the computation of a large number of field points for each field line.

In order to illustrate some of the features of the field line patterns, we consider the simple case of a vertical

dipole for which $\mathbf{u} = \mathbf{e}_z$. Then $\mathbf{u} \cdot \mathbf{e}_\rho = 0$ and $\mathbf{u} \cdot \mathbf{e}_\phi = 0$, and many terms vanish. For the dipole fields in Equations (7) and (8) we have

$$\hat{\mathbf{q}}_1 = \frac{1}{q_1} [\bar{\rho} \mathbf{e}_\rho + (\bar{z} + h) \mathbf{e}_z], \quad (39)$$

with

$$q_1 = \sqrt{\bar{\rho}^2 + (\bar{z} + h)^2}, \quad (40)$$

in cylindrical coordinates. The reflected fields simplify to

$$\tilde{\mathbf{E}}_r(\mathbf{r}) = \mathbf{e}_\rho R_p^{(4)} + \mathbf{e}_z R_p^{(3)}, \quad (41)$$

$$\tilde{\mathbf{B}}_r(\mathbf{r}) = \mathbf{e}_\phi R_p^{(7)}. \quad (42)$$

For the fields in the layer we obtain

$$\tilde{\mathbf{E}}_k(\mathbf{r}) = \mathbf{e}_\rho D_{kp}^{(4)} + \mathbf{e}_z D_{kp}^{(3)}, \quad (43)$$

$$\tilde{\mathbf{B}}_k(\mathbf{r}) = \mathbf{e}_\phi D_{kp}^{(8)}, \quad (44)$$

with $k = a, b$, and the transmitted fields become

$$\tilde{\mathbf{E}}_t(\mathbf{r}) = \mathbf{e}_\rho T_p^{(4)} + \mathbf{e}_z T_p^{(3)}, \quad (45)$$

$$\tilde{\mathbf{B}}_t(\mathbf{r}) = \mathbf{e}_\phi T_p^{(8)}. \quad (46)$$

For a given field point, the electric fields are linear combinations of \mathbf{e}_ρ and \mathbf{e}_z and the magnetic fields are proportional to \mathbf{e}_ϕ . Therefore, the Poynting vector is a linear combination of \mathbf{e}_ρ and \mathbf{e}_z . We now consider a plane which contains the z axis. Vectors \mathbf{e}_ρ and \mathbf{e}_z span this plane, and so the Poynting vector is in this plane. Consequently, a field line through a point in this plane lies entirely in the plane. In general, field lines are three-dimensional curves, but for the case of a vertical dipole the field lines lie in a two-dimensional plane containing the z axis. Moreover, the system is rotation symmetric around the z axis, so without loss of generality we only need to consider the yz plane with $y > 0$.

Figure 6 shows the flow-line pattern for $\varepsilon_1 = 1$, $\varepsilon_2 = 4$, $\varepsilon_3 = 2$, $\mu_1 = \mu_2 = \mu_3 = 1$, $\ell = 3$, and $h = 2$. All field lines emerge from the dipole as approximately straight lines. A field line which hits the $\bar{z} = 0$ interface continues into the layer, and upon entering, its direction changes. This field line bends toward the normal upon transmission, reminiscent of the transmission of an optical ray at such an interface (medium 2 is optically thicker than medium 1). The change in angle, though, does not obey Snell's law, and there is no reflected ray. At the second interface, all field lines continue into medium 3, and their directions bend away from the normal upon transmission. This could be expected, since medium 3 is optically thinner than medium 2.

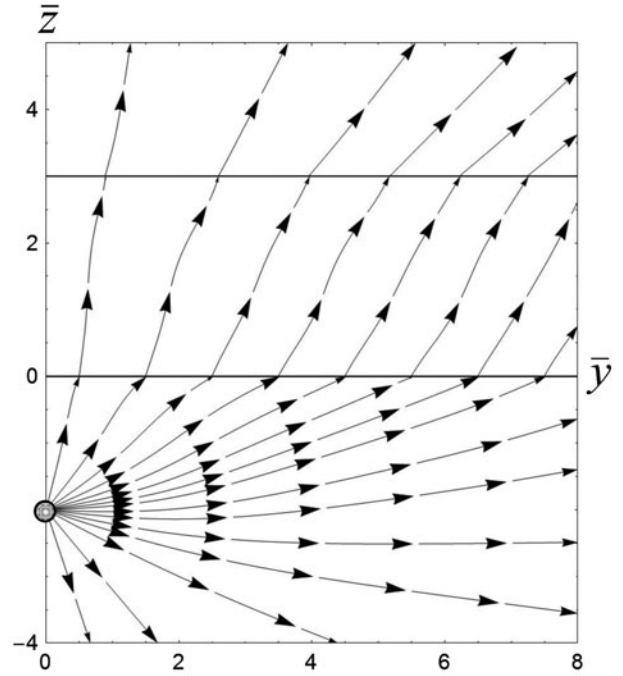


Figure 6. Shown here is the energy flow pattern for radiation emitted by a vertical dipole located on the z axis ($h = 2$). The dimensionless layer thickness is $\ell = 3$ and the two interfaces are shown as solid lines. The material parameters are $\varepsilon_1 = 1$, $\varepsilon_2 = 4$, $\varepsilon_3 = 2$, and all μ are equal to unity.

Figure 7 shows a field line pattern for the same case as in Figure 6, except that $\varepsilon_1 = 4$ and $\varepsilon_2 = 1$. At the $\bar{z} = \ell$ interface, the field lines enter an optically thicker medium, and bend toward the normal, as expected. The behavior near the $\bar{z} = 0$ interface, however, is drastically different than expected. Field lines that approach the interface near the \bar{z} axis continue across the interface, and then slightly bend away from the normal. Field lines

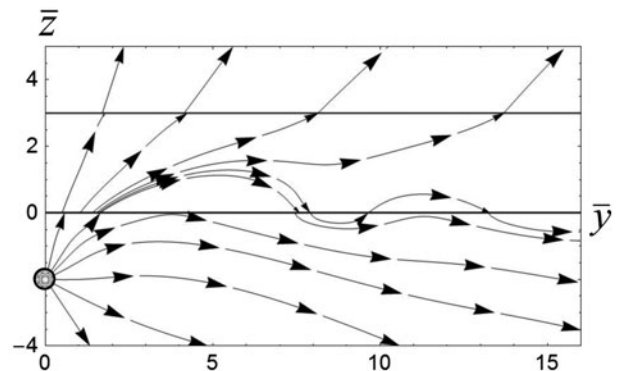


Figure 7. Shown here is the energy flow pattern for $h = 2$, $\ell = 3$, $\varepsilon_1 = 4$, $\varepsilon_2 = 1$, $\varepsilon_3 = 2$, and all μ are equal to unity. The dip of the flow lines below the $\bar{z} = 0$ interface near $\bar{y} = 9$ is shown enlarged in Figure 8.

that cross the interface more to the right in the figure continue in medium 2, but then cross the interface again, returning to medium 1. Thus, the transported energy oscillates back and forth through the interface, and this continues indefinitely (outside the figure). Unlike in Figure 6, where the field lines in medium 1 are approximately straight, here we see that some field lines that run into the direction of the interface change direction when approaching the interface, and then continue downward.

Figure 8 shows an enlargement of a part of Figure 7, near the area where the field lines first dip below the interface. An optical vortex appears just above the interface, where the energy continuously swirls around a singular point, indicated by a little circle. Just above the vortex is another singular point. A bundle of field lines that approaches this point from the left splits at the singularity. Just above and below the singularity, the field lines run in opposite directions. Since the pattern is rotation symmetric around the z axis, these singular points are actually points on a singular circle around the z axis, and the vortex is a torus vortex around the z axis. For larger values of \bar{y} , there is a vortex above every dip of the field lines that drop below the interface. Thus, there is a set of concentric vortex tori just above the interface. At a singularity, the Poynting vector vanishes, and it can be shown that at the center of a vortex this is due to the disappearance of the magnetic field [13]. At a singularity where the field lines split, the Poynting vector is zero because $\vec{E}_i(\mathbf{r})^* \times \vec{B}_i(\mathbf{r})/\mu_i$ is purely imaginary.

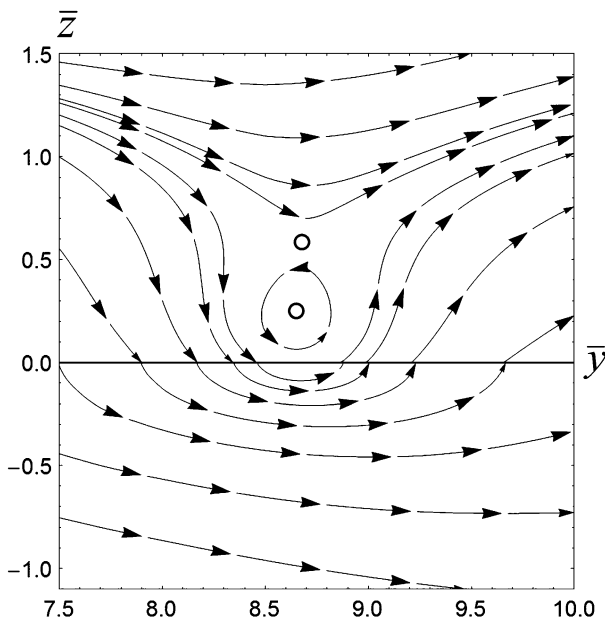


Figure 8. Shown here is an enlargement of a part of the flow pattern of Figure 7. The two white circles denote the singular points.

8. Conclusions

We have considered the arrangement shown in Figure 1 where an oscillating electric dipole, embedded in material, is located near a slab of uniform material. We have obtained the exact solution of Maxwell's equations for this configuration, without any restrictions on the material constants or the state of oscillation of the dipole. This elegant solution, given in Appendix 3, is expressed in a set of auxiliary functions, defined in Appendix 2. These functions depend on the dimensionless cylindrical coordinates $\bar{\rho}$ and \bar{z} of the field point. The integral representations of these auxiliary functions contain the Fresnel coefficients for reflection and transmission of a plane wave, and cylindrical Bessel functions which come from the angular integration in the \mathbf{k}_{\parallel} plane of the angular spectrum solution for the various fields. The integration variable α is the dimensionless magnitude of the \mathbf{k}_{\parallel} vector. The integrands of some of these functions have a singularity at $\alpha = n_1$ (if $n_1 > 0$), which is the borderline between traveling and evanescent waves of the incident field. By splitting these integrals in traveling and evanescent parts, and making a change of variables, these singularities disappear. Moreover, sharp peaks in the Fresnel coefficients at $\alpha = n_1$ are smoothed out by this procedure.

Electromagnetic energy flows along the field lines of the Poynting vector. With the solutions for the electric and magnetic fields, this Poynting vector can be constructed. We have considered the simplest case of a vertical dipole for which the radiation field is rotation symmetric around the z axis, and the field lines of the Poynting vector lie in a plane (rather than being three-dimensional curves). Typical flow patterns are shown in Figures 6 and 7. Field lines appear to emerge from the dipole as nearly straight lines. When the material of the layer is optically thicker than the embedding medium, as in Figure 6, the field lines seem to refract at the first interface, similar to optical rays (although they do not follow Snell's law). However, when the material of the layer is optically thinner than the embedding medium, as in Figure 7, the field lines in both regions, 1 and 2, curve considerably. Many field lines that emerge from the dipole in the upward direction do not reach the interface, but bend downwards after a certain distance. Other field lines cross the interface, but then return back to medium 1. Then they bend again, and cross the interface again. This continues, resulting in a persisting oscillation of energy around the first interface. Once a field line crosses the second interface, it continues as approximately a straight line in medium 3.

Figure 8 shows an enlargement of the flow pattern of Figure 7, in the neighborhood of where the field lines dip below the interface. It appears that close to the interface some of the energy circulates in closed loops around a singular point. Since the system is rotation symmetric around

the z axis, this point actually represents a singular circle. These vortices appear above every point where field lines dip below the interface, leading to a set of concentric torus-shaped vortices in the field line pattern. Above each torus is a singular circle, indicated by a small white circle in Figure 8. This is necessary since just above and below this circle the energy flows in opposite directions.

References

- [1] Sommerfeld, A. *Ann. Phys.* **1909**, 333, 665–736.
- [2] Lukosz, W.; Kunz, R.E. *J. Opt. Soc. Am.* **1977**, 67, 1607–1615.
- [3] Lukosz, W.; Kunz, R.E. *J. Opt. Soc. Am.* **1977**, 67, 1615–1619.
- [4] Sipe, J.E. *Surf. Sci.* **1981**, 105, 489–504.
- [5] Sipe, J.E. *J. Opt. Soc. Am. B* **1987**, 4, 481–489.
- [6] Novotny, L.J. *Opt. Soc. Am. A* **1997**, 14, 91–104.
- [7] Arnoldus, H.F.; Foley, J.T.J. *Opt. Soc. Am. A* **2004**, 21, 1109–1117.
- [8] Drexhage, K.H. In *Progress in Optics*; Wolf, E., Ed.; North-Holland: Amsterdam, 1974; Vol. XII; pp 163–232.
- [9] Lukosz, W.; Kunz, R.E. *Opt. Commun.* **1977**, 20, 195–199.
- [10] Chance, R.R.; Prock, A.; Silbey, R. *Adv. Chem. Phys.* **1978**, 39, 1–65.
- [11] Ford, G.W.; Weber, W.H. *Surf. Sci.* **1981**, 109, 451–481.
- [12] Ford, G.W.; Weber, W.H. *Phys. Rep.* **1984**, 113, 195–287.
- [13] Li, X.; Arnoldus, H.F. *Opt. Commun.* **2013**, 305, 76–81.
- [14] Li, X.; Arnoldus, H.F. *Phys. Rev. A* **2010**, 81, 053844–1–053844–10.
- [15] Arnoldus, H.F.; Berg, M.J.; Li, X. *Phys. Lett. A* **2014**, 378, 755–759.
- [16] Lindell, I.V. *Methods for Electromagnetic Field Analysis*; Oxford University Press, Oxford, 1992; Section 1.4.
- [17] Arnoldus, H.F.; Foley, J.T. *Opt. Commun.* **2004**, 231, 115–128.
- [18] Li, X.; Pierce, D.M.; Arnoldus, H.F.J. *Opt. Soc. Am. A* **2011**, 28, 778–785.
- [19] Novotny, L.; Hecht, B. *Principles of Nano-optics*; Cambridge University Press, New York, 2007; Appendix C.
- [20] Arnoldus, H.F. *Adv. Im. Electr. Phys.* **2004**, 132, 1–67.

Appendix 1. Fresnel coefficients

The fields in the various regions ($i = 1, 2, 3$) are derived from an angular spectrum representation of the incident field. For this construction, we need the solution for an incident plane wave with wave vector \mathbf{k} , given by Equation (10), and polarization σ . The various wave vectors are shown in Figure 2. Due to boundary conditions, all wave vectors must have the same parallel component k_{\parallel} . For each wave vector it has to hold that

$$\mathbf{k}_{\gamma} \cdot \mathbf{k}_{\gamma} = n^2 k_o^2, \quad (\text{A1})$$

where $\gamma = r, a, b$, or t , and the \mathbf{k} vector without a subscript refers to the incident wave, as in Section 3. The index of refraction n is taken as that of the medium in which the wave propagates. Equation (A1) is the dispersion relation for the wave with wave vector \mathbf{k}_{γ} . We consider vector \mathbf{k}_{\parallel} as given, and

therefore only the z components of the wave vectors need to be determined. With Equation (A1) we then have $k_{\gamma z} = \pm k_o v$, and v for medium i is defined as in Equation (12) for $i = 1$. From causality it follows that $k_{rz} = -k_o v_1$ and $k_{tz} = k_o v_3$. For the a and b waves we take $k_{az} = k_o v_2$ and $k_{bz} = -k_o v_2$. The polarization vectors for s polarization are defined by Equation (15), and these are the same for each wave. For p polarization, we define these vectors as

$$\mathbf{e}_{\gamma p} = \frac{1}{nk_o} \mathbf{k}_{\gamma} \times \mathbf{e}_s, \quad (\text{A2})$$

with n being the index of refraction for the corresponding medium.

The electric field of the plane wave in $z < 0$ is written as

$$\mathbf{E}(\mathbf{r}) = E_o e^{i\mathbf{k}_{\parallel} \cdot \mathbf{r}} [\mathbf{e}_{\sigma} \exp(i v_1 \bar{z}) + R_{\sigma} \mathbf{e}_{\sigma} \exp(-i v_1 \bar{z})], \quad (\text{A3})$$

which is the sum of the incident field and the reflected field. Here, we set $\bar{z} = k_o z$, and E_o is an overall factor. For $0 < z < L$ we have

$$\mathbf{E}(\mathbf{r}) = E_o e^{i\mathbf{k}_{\parallel} \cdot \mathbf{r}} \{D_{aa} \mathbf{e}_{a\sigma} \exp(i v_2 \bar{z}) + D_{ba} \mathbf{e}_{b\sigma} \exp[i v_2 (\ell - \bar{z})]\}, \quad (\text{A4})$$

and for $z > L$ the field is

$$\mathbf{E}(\mathbf{r}) = E_o e^{i\mathbf{k}_{\parallel} \cdot \mathbf{r}} T_{\sigma} \mathbf{e}_{i\sigma} \exp[i v_3 (\bar{z} - \ell)]. \quad (\text{A5})$$

The magnetic field in each region follows from Equation (14).

The unknowns in the fields in the various regions are the Fresnel coefficients R_{σ} , D_{aa} , D_{ba} , and T_{σ} . The boundary conditions require that $\varepsilon \mathbf{E}_{\perp}$, \mathbf{E}_{\parallel} , \mathbf{B}_{\perp} , and $\mathbf{B}_{\parallel}/\mu$ are continuous across the boundaries $z = 0$ and $z = L$. For each polarization, this gives eight equations for the four unknown Fresnel coefficient. Upon solving these, we find for s polarization

$$R_s(\alpha) = \frac{1}{\Lambda_s} [(\mu_2 v_1 - \mu_1 v_2)(\mu_3 v_2 + \mu_2 v_3) + (\mu_2 v_1 + \mu_1 v_2)(\mu_3 v_2 - \mu_2 v_3) \exp(2i v_2 \ell)], \quad (\text{A6})$$

$$D_{as}(\alpha) = \frac{2}{\Lambda_s} \mu_2 v_1 (\mu_3 v_2 + \mu_2 v_3), \quad (\text{A7})$$

$$D_{bs}(\alpha) = \frac{2}{\Lambda_s} \mu_2 v_1 (\mu_3 v_2 - \mu_2 v_3) \exp(i v_2 \ell), \quad (\text{A8})$$

$$T_s(\alpha) = \frac{4}{\Lambda_s} \mu_2 \mu_3 v_1 v_2 \exp(i v_2 \ell), \quad (\text{A9})$$

with

$$\Lambda_s = (\mu_2 v_1 + \mu_1 v_2)(\mu_3 v_2 + \mu_2 v_3) + (\mu_2 v_1 - \mu_1 v_2)(\mu_3 v_2 - \mu_2 v_3) \exp(2i v_2 \ell). \quad (\text{A10})$$

The α dependence enters through the functions v_i . For p polarization we obtain

$$R_p(\alpha) = \frac{1}{\Lambda_p} [(\varepsilon_2 v_1 - \varepsilon_1 v_2)(\varepsilon_3 v_2 + \varepsilon_2 v_3) + (\varepsilon_2 v_1 + \varepsilon_1 v_2)(\varepsilon_3 v_2 - \varepsilon_2 v_3) \exp(2i v_2 \ell)], \quad (\text{A11})$$

$$D_{ap}(\alpha) = \frac{2}{\Lambda_p n_1} n_2 \varepsilon_1 v_1 (\varepsilon_3 v_2 + \varepsilon_2 v_3), \quad (\text{A12})$$

$$D_{bp}(\alpha) = \frac{2}{\Lambda_p n_1} n_2 \varepsilon_1 v_1 (\varepsilon_3 v_2 - \varepsilon_2 v_3) \exp(iv_2 \ell), \quad (\text{A13})$$

$$T_p(\alpha) = \frac{4}{\Lambda_p n_1} n_3 \varepsilon_1 \varepsilon_2 v_1 v_2 \exp(iv_2 \ell), \quad (\text{A14})$$

with

$$\Lambda_p = (\varepsilon_2 v_1 + \varepsilon_1 v_2)(\varepsilon_3 v_2 + \varepsilon_2 v_3) + (\varepsilon_2 v_1 - \varepsilon_1 v_2)(\varepsilon_3 v_2 - \varepsilon_2 v_3) \exp(2iv_2 \ell). \quad (\text{A15})$$

Appendix 2. Auxiliary functions

The electric and magnetic fields are computed with the method outlined in Section 4, and the result can be expressed in terms of a set of auxiliary functions. First, we define the associated functions

$$r_\sigma(\alpha, \bar{z}) = R_\sigma \exp[iv_1(h - \bar{z})], \quad (\text{B1})$$

$$d_{a\sigma}(\alpha, \bar{z}) = \frac{1}{v_1} D_{a\sigma} \exp(iv_1 h + iv_2 \bar{z}), \quad (\text{B2})$$

$$d_{b\sigma}(\alpha, \bar{z}) = \frac{1}{v_1} D_{b\sigma} \exp[iv_1 h + iv_2(\ell - \bar{z})], \quad (\text{B3})$$

$$t_\sigma(\alpha, \bar{z}) = \frac{1}{v_1} T_\sigma \exp[iv_1 h + iv_3(\bar{z} - \ell)], \quad (\text{B4})$$

which contain the Fresnel coefficients from Appendix 1. These functions depend on the field-point coordinate \bar{z} and the integration variable α . Angular spectra representations have the characteristic $1/v_1$ singularity, as can be seen from Equation (13). However, all Fresnel coefficients, except R_s and R_p , are proportional to v_1 , so in the associated functions this factor cancels.

The auxiliary functions for s -polarized waves are

$$R_s^{(1)}(\bar{\rho}, \bar{z}) = \frac{i}{2} \int_0^\infty d\alpha \alpha r_s \frac{1}{v_1} (J_0 + J_2), \quad (\text{B5})$$

$$R_s^{(2)}(\bar{\rho}, \bar{z}) = \frac{i}{2} \int_0^\infty d\alpha \alpha r_s \frac{1}{v_1} (J_0 - J_2), \quad (\text{B6})$$

$$R_s^{(3)}(\bar{\rho}, \bar{z}) = \frac{i}{2} \int_0^\infty d\alpha \alpha r_s (J_0 - J_2), \quad (\text{B7})$$

$$R_s^{(4)}(\bar{\rho}, \bar{z}) = -\frac{i}{2} \int_0^\infty d\alpha \alpha r_s (J_0 + J_2), \quad (\text{B8})$$

$$R_s^{(5)}(\bar{\rho}, \bar{z}) = -\int_0^\infty d\alpha \alpha r_s \frac{\alpha}{v_1} J_1, \quad (\text{B9})$$

$$D_{as}^{(1)}(\bar{\rho}, \bar{z}) = \frac{i}{2} \int_0^\infty d\alpha \alpha d_{as} (J_0 + J_2), \quad (\text{B10})$$

$$D_{as}^{(2)}(\bar{\rho}, \bar{z}) = \frac{i}{2} \int_0^\infty d\alpha \alpha d_{as} (J_0 - J_2), \quad (\text{B11})$$

$$D_{as}^{(3)}(\bar{\rho}, \bar{z}) = -\frac{i}{2} \int_0^\infty d\alpha \alpha d_{as} v_2 (J_0 - J_2), \quad (\text{B12})$$

$$D_{as}^{(4)}(\bar{\rho}, \bar{z}) = \frac{i}{2} \int_0^\infty d\alpha \alpha d_{as} v_2 (J_0 + J_2), \quad (\text{B13})$$

$$D_{as}^{(5)}(\bar{\rho}, \bar{z}) = -\int_0^\infty d\alpha \alpha d_{as} \alpha J_1, \quad (\text{B14})$$

$$D_{bs}^{(1)}(\bar{\rho}, \bar{z}) = \frac{i}{2} \int_0^\infty d\alpha \alpha d_{bs} (J_0 + J_2), \quad (\text{B15})$$

$$D_{bs}^{(2)}(\bar{\rho}, \bar{z}) = \frac{i}{2} \int_0^\infty d\alpha \alpha d_{bs} (J_0 - J_2), \quad (\text{B16})$$

$$D_{bs}^{(3)}(\bar{\rho}, \bar{z}) = \frac{i}{2} \int_0^\infty d\alpha \alpha d_{bs} v_2 (J_0 - J_2), \quad (\text{B17})$$

$$D_{bs}^{(4)}(\bar{\rho}, \bar{z}) = -\frac{i}{2} \int_0^\infty d\alpha \alpha d_{bs} v_2 (J_0 + J_2), \quad (\text{B18})$$

$$D_{bs}^{(5)}(\bar{\rho}, \bar{z}) = -\int_0^\infty d\alpha \alpha d_{bs} \alpha J_1, \quad (\text{B19})$$

$$T_s^{(1)}(\bar{\rho}, \bar{z}) = \frac{i}{2} \int_0^\infty d\alpha \alpha t_s (J_0 + J_2), \quad (\text{B20})$$

$$T_s^{(2)}(\bar{\rho}, \bar{z}) = \frac{i}{2} \int_0^\infty d\alpha \alpha t_s (J_0 - J_2), \quad (\text{B21})$$

$$T_s^{(3)}(\bar{\rho}, \bar{z}) = -\frac{i}{2} \int_0^\infty d\alpha \alpha t_s v_3 (J_0 - J_2), \quad (\text{B22})$$

$$T_s^{(4)}(\bar{\rho}, \bar{z}) = \frac{i}{2} \int_0^\infty d\alpha \alpha t_s v_3 (J_0 + J_2), \quad (\text{B23})$$

$$T_s^{(5)}(\bar{\rho}, \bar{z}) = -\int_0^\infty d\alpha \alpha t_s \alpha J_1, \quad (\text{B24})$$

and for p -polarized waves we have

$$R_p^{(1)}(\bar{\rho}, \bar{z}) = -\frac{i}{2n_1^2} \int_0^\infty d\alpha \alpha r_p v_1 (J_0 - J_2), \quad (\text{B25})$$

$$R_p^{(2)}(\bar{\rho}, \bar{z}) = -\frac{i}{2n_1^2} \int_0^\infty d\alpha \alpha r_p v_1 (J_0 + J_2), \quad (\text{B26})$$

$$R_p^{(3)}(\bar{\rho}, \bar{z}) = \frac{i}{n_1^2} \int_0^\infty d\alpha \alpha r_p \frac{\alpha^2}{v_1} J_0, \quad (\text{B27})$$

$$R_p^{(4)}(\bar{\rho}, \bar{z}) = -\frac{1}{n_1^2} \int_0^\infty d\alpha \alpha r_p \alpha J_1, \quad (\text{B28})$$

$$R_p^{(5)}(\bar{\rho}, \bar{z}) = -\frac{i}{2} \int_0^\infty d\alpha \alpha r_p (J_0 + J_2), \quad (\text{B29})$$

$$R_p^{(6)}(\bar{\rho}, \bar{z}) = \frac{i}{2} \int_0^\infty d\alpha \alpha r_p (J_0 - J_2), \quad (\text{B30})$$

$$R_p^{(7)}(\bar{\rho}, \bar{z}) = \int_0^\infty d\alpha \alpha r_p \frac{\alpha}{v_1} J_1, \quad (\text{B31})$$

$$D_{ap}^{(1)}(\bar{\rho}, \bar{z}) = \frac{i}{2n_1 n_2} \int_0^\infty d\alpha \alpha d_{ap} v_1 v_2 (J_0 - J_2), \quad (\text{B32})$$

$$D_{ap}^{(2)}(\bar{\rho}, \bar{z}) = \frac{i}{2n_1 n_2} \int_0^\infty d\alpha \alpha d_{ap} v_1 v_2 (J_0 + J_2), \quad (\text{B33})$$

$$D_{ap}^{(3)}(\bar{\rho}, \bar{z}) = \frac{i}{n_1 n_2} \int_0^\infty d\alpha \alpha d_{ap} \alpha^2 J_0, \quad (\text{B34})$$

$$D_{ap}^{(4)}(\bar{\rho}, \bar{z}) = \frac{1}{n_1 n_2} \int_0^\infty d\alpha \alpha d_{ap} \alpha v_2 J_1, \quad (\text{B35})$$

$$D_{ap}^{(5)}(\bar{\rho}, \bar{z}) = \frac{1}{n_1 n_2} \int_0^\infty d\alpha \alpha d_{ap} \alpha v_1 J_1, \quad (\text{B36})$$

$$D_{ap}^{(6)}(\bar{\rho}, \bar{z}) = -\frac{in_2}{2n_1} \int_0^\infty d\alpha \alpha d_{ap} v_1 (J_0 + J_2), \quad (\text{B37})$$

$$D_{ap}^{(7)}(\bar{\rho}, \bar{z}) = \frac{in_2}{2n_1} \int_0^\infty d\alpha \alpha d_{ap} v_1 (J_0 - J_2), \quad (\text{B38})$$

$$D_{ap}^{(8)}(\bar{\rho}, \bar{z}) = \frac{n_2}{n_1} \int_0^\infty d\alpha \alpha d_{ap} \alpha J_1, \quad (\text{B39})$$

$$D_{bp}^{(1)}(\bar{\rho}, \bar{z}) = -\frac{i}{2n_1 n_2} \int_0^\infty d\alpha \alpha d_{bp} v_1 v_2 (J_0 - J_2), \quad (\text{B40})$$

$$D_{bp}^{(2)}(\bar{\rho}, \bar{z}) = -\frac{i}{2n_1 n_2} \int_0^\infty d\alpha \alpha d_{bp} v_1 v_2 (J_0 + J_2), \quad (\text{B41})$$

$$D_{bp}^{(3)}(\bar{\rho}, \bar{z}) = \frac{i}{n_1 n_2} \int_0^\infty d\alpha \alpha d_{bp} \alpha^2 J_0, \quad (\text{B42})$$

$$D_{bp}^{(4)}(\bar{\rho}, \bar{z}) = -\frac{1}{n_1 n_2} \int_0^\infty d\alpha \alpha d_{bp} \alpha v_2 J_1, \quad (\text{B43})$$

$$D_{bp}^{(5)}(\bar{\rho}, \bar{z}) = \frac{1}{n_1 n_2} \int_0^\infty d\alpha \alpha d_{bp} \alpha v_1 J_1, \quad (\text{B44})$$

$$D_{bp}^{(6)}(\bar{\rho}, \bar{z}) = -\frac{in_2}{2n_1} \int_0^\infty d\alpha \alpha d_{bp} v_1 (J_0 + J_2), \quad (\text{B45})$$

$$D_{bp}^{(7)}(\bar{\rho}, \bar{z}) = \frac{in_2}{2n_1} \int_0^\infty d\alpha \alpha d_{bp} v_1 (J_0 - J_2), \quad (\text{B46})$$

$$D_{bp}^{(8)}(\bar{\rho}, \bar{z}) = \frac{n_2}{n_1} \int_0^\infty d\alpha \alpha d_{bp} \alpha J_1, \quad (\text{B47})$$

$$T_p^{(1)}(\bar{\rho}, \bar{z}) = \frac{i}{2n_1 n_3} \int_0^\infty d\alpha \alpha t_p v_1 v_3 (J_0 - J_2), \quad (\text{B48})$$

$$T_p^{(2)}(\bar{\rho}, \bar{z}) = \frac{i}{2n_1 n_3} \int_0^\infty d\alpha \alpha t_p v_1 v_3 (J_0 + J_2), \quad (\text{B49})$$

$$T_p^{(3)}(\bar{\rho}, \bar{z}) = \frac{i}{n_1 n_3} \int_0^\infty d\alpha \alpha t_p \alpha^2 J_0, \quad (\text{B50})$$

$$T_p^{(4)}(\bar{\rho}, \bar{z}) = \frac{1}{n_1 n_3} \int_0^\infty d\alpha \alpha t_p \alpha v_3 J_1, \quad (\text{B51})$$

$$T_p^{(5)}(\bar{\rho}, \bar{z}) = \frac{1}{n_1 n_3} \int_0^\infty d\alpha \alpha t_p \alpha v_1 J_1, \quad (\text{B52})$$

$$T_p^{(6)}(\bar{\rho}, \bar{z}) = -\frac{in_3}{2n_1} \int_0^\infty d\alpha \alpha t_p v_1 (J_0 + J_2), \quad (\text{B53})$$

$$T_p^{(7)}(\bar{\rho}, \bar{z}) = \frac{in_3}{2n_1} \int_0^\infty d\alpha \alpha t_p v_1 (J_0 - J_2), \quad (\text{B54})$$

$$T_p^{(8)}(\bar{\rho}, \bar{z}) = \frac{n_3}{n_1} \int_0^\infty d\alpha \alpha t_p \alpha J_1. \quad (\text{B55})$$

The argument of each Bessel function is $\alpha\bar{\rho}$. The auxiliary functions depend on $\bar{\rho}$ through the arguments of the Bessel functions and on \bar{z} through the \bar{z} dependence of the associated functions. All integrands have a factor of α . We could have simplified the notation by absorbing this α in the associated functions, but the combination $\alpha d\alpha$ is more convenient for splitting the integrals into traveling and evanescent parts, as shown in Section 5.

Appendix 3. Electric and magnetic fields

With the method outlined in Section 4, the electric and magnetic fields can be obtained. We use cylindrical coordinates (ρ, ϕ, z) for the field point \mathbf{r} . The corresponding basis vectors are \mathbf{e}_ρ , \mathbf{e}_ϕ , and \mathbf{e}_z , and \mathbf{u} is the unit vector representing the state of oscillation of the dipole. We obtain for the reflected fields

$$\begin{aligned} \vec{E}_r(\mathbf{r}) = & \mathbf{e}_\rho (\mathbf{u} \cdot \mathbf{e}_\rho) (R_s^{(1)} + R_p^{(1)}) + \mathbf{e}_\phi (\mathbf{u} \cdot \mathbf{e}_\phi) \\ & \times (R_s^{(2)} + R_p^{(2)}) + \mathbf{e}_z (\mathbf{u} \cdot \mathbf{e}_z) R_p^{(3)} \\ & + [\mathbf{e}_\rho (\mathbf{u} \cdot \mathbf{e}_z) - \mathbf{e}_z (\mathbf{u} \cdot \mathbf{e}_\rho)] R_p^{(4)}, \end{aligned} \quad (\text{C1})$$

$$\begin{aligned} \tilde{\mathbf{B}}_r(\mathbf{r}) = & \mathbf{e}_\rho(\mathbf{u} \cdot \mathbf{e}_\phi)(R_s^{(3)} + R_p^{(5)}) + \mathbf{e}_\phi(\mathbf{u} \cdot \mathbf{e}_\rho)(R_s^{(4)} + R_p^{(6)}) \\ & + \mathbf{e}_z(\mathbf{u} \cdot \mathbf{e}_\phi)R_s^{(5)} + \mathbf{e}_\phi(\mathbf{u} \cdot \mathbf{e}_z)R_p^{(7)}. \end{aligned} \quad (\text{C2})$$

The fields in the layer are

$$\begin{aligned} \tilde{\mathbf{E}}_k(\mathbf{r}) = & \mathbf{e}_\rho(\mathbf{u} \cdot \mathbf{e}_\rho)(D_{ks}^{(1)} + D_{kp}^{(1)}) + \mathbf{e}_\phi(\mathbf{u} \cdot \mathbf{e}_\phi) \\ & \times (D_{ks}^{(2)} + D_{kp}^{(2)}) + (\mathbf{u} \cdot \mathbf{e}_z)(\mathbf{e}_z D_{kp}^{(3)} + \mathbf{e}_\rho D_{kp}^{(4)}) \\ & + \mathbf{e}_z(\mathbf{u} \cdot \mathbf{e}_\rho)D_{kp}^{(5)}, \end{aligned} \quad (\text{C3})$$

$$\begin{aligned} \tilde{\mathbf{B}}_k(\mathbf{r}) = & \mathbf{e}_\rho(\mathbf{u} \cdot \mathbf{e}_\phi)(D_{ks}^{(3)} + D_{kp}^{(6)}) + \mathbf{e}_\phi(\mathbf{u} \cdot \mathbf{e}_\rho) \\ & \times (D_{ks}^{(4)} + D_{kp}^{(7)}) + \mathbf{e}_z(\mathbf{u} \cdot \mathbf{e}_\phi)D_{ks}^{(5)} \\ & + \mathbf{e}_\phi(\mathbf{u} \cdot \mathbf{e}_z)D_{kp}^{(8)}, \end{aligned} \quad (\text{C4})$$

with $k = a, b$, and the transmitted fields are

$$\begin{aligned} \tilde{\mathbf{E}}_t(\mathbf{r}) = & \mathbf{e}_\rho(\mathbf{u} \cdot \mathbf{e}_\rho)(T_s^{(1)} + T_p^{(1)}) + \mathbf{e}_\phi(\mathbf{u} \cdot \mathbf{e}_\phi)(T_s^{(2)} + T_p^{(2)}) \\ & + (\mathbf{u} \cdot \mathbf{e}_z)(\mathbf{e}_z T_p^{(3)} + \mathbf{e}_\rho T_p^{(4)}) + \mathbf{e}_z(\mathbf{u} \cdot \mathbf{e}_\rho)T_p^{(5)}, \end{aligned} \quad (\text{C5})$$

$$\begin{aligned} \tilde{\mathbf{B}}_t(\mathbf{r}) = & \mathbf{e}_\rho(\mathbf{u} \cdot \mathbf{e}_\phi)(T_s^{(3)} + T_p^{(6)}) + \mathbf{e}_\phi(\mathbf{u} \cdot \mathbf{e}_\rho)(T_s^{(4)} + T_p^{(7)}) \\ & + \mathbf{e}_z(\mathbf{u} \cdot \mathbf{e}_\phi)T_s^{(5)} + \mathbf{e}_\phi(\mathbf{u} \cdot \mathbf{e}_z)T_p^{(8)}. \end{aligned} \quad (\text{C6})$$